Published in final edited form as:
Life Sci. 2012 June 27; 90(25-26): 1001–1009. doi:10.1016/j.lfs.2012.05.016.

Altered adipocyte progenitor population and adipose-related gene profile in adipose tissue by long-term high-fat diet in mice

Xiaohua Xu[a], **Cuiqing Liu**[b,c], **Zhaobin Xu**[a], **Kevin Tzan**[a], **Aixia Wang**[b], **Sanjay Rajagopalan**[b,d], and **Qinghua Sun**[a,b,d]

[a]Division of Environmental Health Sciences, College of Public Health, The Ohio State University, Columbus, OH 43210, United States

[b]Davis Heart and Lung Research Institute, The Ohio State University, Columbus, OH 43210, United States

[c]Department of Physiology, Hangzhou Normal University, Hangzhou, China

[d]Division of Cardiology, College of Medicine, The Ohio State University, Columbus, OH 43210, United States

Abstract

Aims—High-fat diet (HFD) is associated with adipose inflammation, which contributes to key components of metabolic abnormalities. The expanded adipose tissue mass associated with obesity is the result of hyperplasia and hypertrophy of adipocytes. In this study, we investigated the effects of long-term HFD on adipocyte progenitor cell (APC) population and adipose-specific gene profiles in both white and brown adipose, and the role of perivascular adipose in the alteration of vascular function in response to HFD.

Main methods—Male C57BL/6 mice were fed a standard normal diet (ND) or HFD for about 8 months. Glucose metabolism was assessed by an intraperitoneal glucose tolerance test. APC population and adipose-related gene profile were evaluated, and vascular function was measured in the presence or absence of perivascular adipose. Adiponectin and AMPK activity were also investigated.

Key findings—HFD induced insulin resistance and glucose intolerance, and resulted in a decrease in APC population in brown, but not in white adipose tissue, when compared with animals fed a ND, with differential alterations of white and brown adipocyte-specific gene expression in brown and white adipose. Additionally, HFD led to altered vascular function in arteries in the presence of perivascular adipose tissue, which is associated with increased superoxide production. Adiponectin and AMPK activity were significantly decreased in response to long-term HFD.

Significance—These findings suggest that long-term high-fat intake differentially alters adipocyte progenitor population and adipose-related gene expression in adipose tissue, and adiponectin-AMPK signaling might be involved. In addition, HFD induces changes in perivascular adipose-mediated vascular function.

Address correspondence to: Qinghua Sun, M.D., Ph.D., Division of Environmental Health Sciences, 396 Biomedical Research Tower, 460 West 12th Avenue, Columbus, OH 43210, United States. Phone: (614) 247-1560; Fax: (614) 688-4233; sun.224@osu.edu.

Keywords

insulin resistance; obesity; adipocyte progenitor cells; vascular function; AMPK

Introduction

Obesity is a global health problem which jeopardizes human health because it has been implicated in the development of type 2 diabetes, hepatic steatosis, cardiovascular diseases, and decreased longevity. Despite the clinical importance of obesity, understanding its development in vivo is extremely limited. It is well known that besides the increase in the size of individual adipocytes, the generation of new adipocytes was the intriguing reason for increased adipose mass in obesity (Lane and Tang, 2005). Since the mature adipocytes are postmitotic, some adipocyte progenitor cells (APC) are required for the increase in adipose mass in adult obesity (Rodeheffer et al., 2008). However, the effect of high-fat diet (HFD) on APC in vivo is still poorly understood.

White adipose tissue (WAT) is the primary site of energy storage, while brown adipose tissue (BAT) is specialized for energy expenditure (Spiegelman and Flier, 2001). The physiological role of BAT is to metabolize fatty acids and generate heat (Spiegelman and Flier, 2001). Due to these functional differences, the balance between WAT and BAT affects systemic energy balance and may contribute to the development of obesity. Thus, another explanation for the development of obesity is reduced thermogenic activity in brown adipose tissue (BAT) (Himms-Hagen, 1983). Nonshivering thermogenesis in BAT, which is stimulated by exposure to cold and HFD, serves to regulate body temperature and body weight (Rippe et al., 2000; Rothwell and Stock, 1979). Uncoupling protein 1 (UCP1), specifically expressed in the mitochondrial inner membrane of BAT, generates heat by uncoupling the oxidative phosphorylation, thus playing a pivotal role in thermogenesis (Ricquier, 1999). In spite of significant role of UCP1, its expression in response to HFD is still controversial (Fromme and Klingenspor, 2011).

Emerging studies showed that perivascular adipose tissue not only provides structural support for arteries, it also functions as an endocrine organ, which is able to signal locally and systemically, and as a paracrine tissue that can modulate the function of arterial vascular tone by blunting constriction in response to some vasoactive substances (Gao et al., 2006; Lohn et al., 2002). It is thought that perivascular fat mediated vascular dysfunction and remodeling in pathological situation (Ma et al.; Reifenberger et al., 2007; Verhagen and Visseren, 2011). The effect of HFD on adipose tissue mediated vascular function merits further investigation.

On the basis of these observations, this study focused on the effect of diet intervention on different adipose depots and was designed to test whether APC number contributes to increased adipose mass, to detect UCP1 and other adipose-related genes expression in brown/white adipose tissue in response to a HFD, to investigate the possible signaling pathway involved, and to examine the role of perivascular adipose tissue on vascular function in a model of diet-induced obesity.

Materials and methods

Animals

Six-week-old male C57BL/6 mice (The Jackson Laboratories, Bar Harbor, ME) were equilibrated for 1 week before being fed HFD containing 42% of calories from fat (TD. 88137, Harlan, Madison, WI) or standard normal diet (ND) containing 17% of calories from

fat (7912, Harlan) for 34 weeks (~8 months). All mice were maintained in a climate controlled facility on a 12-h light/12-h dark cycle with free access to water and food. The Committees on Use and Care of Animals of The Ohio State University approved all experimental procedures.

Measures of glucose homeostasis and sample collection

Mice were fasted overnight and intraperitoneal glucose tolerance test (IPGTT) was performed as previously described (Xu et al., 2010). Briefly, Blood glucose levels were measured with an Contour Blood Glucose Meter (Bayer, Mishawaka, IN) at 0, 30, 60, 90, and 120 minutes after intraperitoneal injection of glucose (2 mg/kg body weight). The homeostasis model assessment of the IR index (HOMA-IR) was also calculated as described previously (Xu et al., 2010). At the end of experiment, the interscapular epididymal, retroperitoneal, inguinal adipose tissues and heart were harvested, weighed, and immediately frozen in liquid nitrogen.

Adiponectin measurement

At the end of the study, blood samples were collected and spun, and serum was stored at −80°C for the analysis of adiponectin. Liver and adipose tissue were homogenized, and protein concentration was determined with the BCA assay (Pierce Chemical Co.). Adiponectin in serum, liver and adipose tissue homogenates were measured by using an adiponectin quantification kit (Abcam, Cambridge, MA) following the manufacturer's instructions.

Vascular function study

Thoracic aorta with adhesive tissue were dissected out and placed in a dissecting dish filled with ice-cold oxygenated Krebs solution containing 119 mM NaCl, 4.7 mM KCl, 25 mM $NaHCO_3$, 2.5 mM $CaCl_2$, 1 mM $MgCl_2$, 1.2 mM KH_2PO_4, and 11 mM D-glucose. After careful removal of adhering connective tissue, artery was cut into 2 mm-length ring segments. In some rings the adhering perivascular fat was kept intact intentionally. The ring was suspended between two stainless bins in a 5-ml chamber on a Multi Myograph (Danish, Myo Technology A/S, Denmark) as previously described (Liu et al., 2009; Sun et al., 2008). Krebs solution in the bathing chamber was constantly bubbled with 95% O_2 –5% CO_2 and maintained at 37°C (pH 7.4). Following 60 minutes equilibration, each ring was stretched to 5 mN, a previously determined optimal resting tone for the development of isometric constriction. After arterial contractility was tested, phenylephrine (1 μM, submaximal concentration) was used to contract the rings with and without adhesive fat. The relaxing effect of acetylcholine (30 nM–10 μM) was studied and compared with the control. The rings were then rinsed in pre-warmed, oxygenated Krebs solution several times until a stable resting tone returned and finally equilibrated for 60 min. The resting tone was readjusted to 5mN if necessary. And then, phenylephrine (30 nM –10 μM) -induced constriction was tested.

Localization and quantification of superoxide production by dihydroethidium in aorta

The oxidative fluorescent probe dihydroethidium (DHE) was used to evaluate in situ superoxide (O_2^-) production on tissue sections. DHE is a cell permeable dye that is oxidized by O_2^- to ethidium bromide, which subsequently intercalates with DNA and is trapped within cell nuclei (Conklin et al., 2004). Frozen aortic segments were cut into 10-μm thick sections. DHE (10 μM, Molecular Probes, Invitrogen) was topically applied to each tissue section. Slides were incubated in a light-protected humidified chamber at room temperature for 30 min, rinsed with phosphate buffered saline, and analyzed with a fluorescent Nikon Eclipse FN1 microscope (Nikon, Tokyo, Japan). Acquisition settings of the camera were

identical for imaging all the sections. Automatic computer-based analysis was performed using MetaMorph software. Fluorescent intensity was quantified in grayscale images under identical imaging conditions by automated detection of the percentage area of each image above baseline image intensity (Wainwright et al., 2006).

Identification of adipose progenitor cells

The APC population was analyzed by flow cytometry as described elsewhere (Rodeheffer et al., 2008). Briefly, interscapular (brown) adipose tissue was digested in Dulbecco's modified Eagle's medium (DMEM) containing 10% fetal bovine serum (FBS), 1% penicillin-streptomycin, and a combination of collagenase type I (1 mg/ml) and collagenase type II (2 mg/ml) at 37°C for 45 minutes with constant stirring. The stromal vascular fraction (SVF) cells from epididymal adipose tissue were isolated as described previously (Sun et al., 2009). The isolated SVF cells were incubated with one of the following directly coupled antibodies: TER119-APC/Cy7, Sca-1-APC, CD34-PE, CD24-PerCP/Cy5.5, CD31-PE/Cy7, and CD29-fluorescein isothiocyanate (FITC) from BioLegend (San Diego, CA); and CD45-PE/Texas red from Invitrogen (Carlsbad, CA) at 4°C for 30 minutes. Cells were analyzed on a LSR II flow cytometer (BD Biosciences). As negative controls, cell aliquots were incubated with isotype-matched rat IgGs or Armenian hamster IgGs under the same conditions.

RNA isolation and quantitative real-time PCR

For gene expression analysis, total RNA was isolated with Trizol (Invitrogen) according to the manufacturer's protocol. Quantitative real-time PCR was performed by the SYBR Green system (Applied Biosystems). Briefly, RNA from interscapular, epididymal, retroperitoneal, and inguinal adipose depots was reversely transcribed using High Capacity cDNA Transcription kit (Invitrogen). Real-time PCR was performed in duplicate using the lightcycler 480 (Roche). The expression level for each gene was calculated using the ΔCt method relative to β-actin. The sequences of all primers used are listed in Table 1.

Western blot analysis

Liver and adipose tissue depots were homogenized with M-PER Mammalian protein extraction reagent (Thermo Scientific) on ice. Equal quantities of tissue protein were separated by 10% SDS-PAGE, and then transferred to immobilon-P polyvinylidene difluoride (PVDF) membrane (Bio-Rad, Hercules, CA). The membranes were immunoblotted with antibody against UCP1 (1:5000, Abcam), AMP-activated protein kinase (AMPK) α (1:500, Cell Signaling) or phospho-AMPKα (1:1000, Cell Signaling) overnight at 4°C, followed by incubated with horseradish peroxidase (HRP)-conjugated goat anti-rabbit IgG (Santa Cruz). The bands were visualized with enhanced chemiluminescence, and the autoradiograph was quantitated by densitometric analysis with Quantity One (Bio-Rad Laboratories) software. Beta-actin was used as a loading control reference.

Immunohistochemistry

Cryosections (10 μm) of mouse brown adipose tissue (interscapular fat) were fixed in a cold acetone for 10 min, followed by treating with 0.3% hydrogen peroxide at room temperature for 10 minutes. After rinsing, the sections were blocked with 1% BSA in PBS and then incubated with rabbit anti-mouse UCP1 (Abcam, 1:300) at 4°C overnight. The sections were incubated with HRP-conjugated goat anti-rabbit IgG (Santa Cruz) at room temperature for 2 hours, and then developed using Fast 3,3′-diaminobenzidine tablet sets (D4293; Sigma-Aldrich) according to the manufacturer's instruction. Counter-staining on nucleus was performed with haematoxylin. After dehydration, the sections were mounted with Permount®. Negative control was performed in the absence of primary antibody. All

measurements were conducted in a double-blinded manner by two independent investigators.

Statistical analysis

Data are expressed as mean ± s.e., unless otherwise indicated. For responses measured repeatedly at different time-points or dose levels, a series of 2-sample independent Student's *t* tests were used to detect the differences between the ND and HFD groups at every time point and dose level, with the Bonferroni correction for multiple comparison adjustment. Comparisons of other continuous variables were conducted with an independent 2-sample Student *t* test, with values of $p < 0.05$ considered significant.

Results

Body weight, fat content, and glucose homeostasis

C57BL/6 mice fed a HFD became more obese and gained ~50% body weight than mice fed a ND (Fig. 1A). There were no significant differences in heart weight between these two groups (Fig. 1B). As shown in Fig. 1C, there was a significant increase in epididymal, retroperitoneal and inguinal fat mass in the animals under HFD, but not in interscapular fat mass. The data from IPGTT indicated that the impairment of glucose tolerance was only concomitant with HFD (Fig. 2A–B). In mice fed a HFD, significant elevations in plasma insulin level (Fig. 2C) and insulin resistance were shown as evaluated by HOMA-IR indexes (Fig. 2D).

APC population changes in response to high-fat diet

Based on that the SVF cells can differentiate into several lineages, including adipocytes named adipocyte-derived stem cells, it is essential to indentify the APC population. The SVF from animals fed a ND or HFD were fractionated and flow cytometry was performed for the isolation of distinct cell populations on the basis of the differential expression of characterized cell-surface markers expressed by stem cell populations. Cells expressing Lin^-:$CD34^+$:$CD29^+$: Sca-1^+:$CD24^+$ was recognized as APC (Rodeheffer et al., 2008). As shown in Fig. 3A–B, a significant decrease in APC number was observed in SVF of brown adipose tissue from mice fed a HFD (BAT: 0.430 ± 0.132% of the cells in the SVF) compared with mice fed a ND (0.938 ± 0.062%). Nonetheless, as shown in Fig. 3C–D, we did not find any significant difference in APC number in white adipose tissue between animals with different diet (ND: 0.583 ± 0.201% *vs.* HFD: 0.543 ± 0.503%). We then wanted to know if HFD selectively decreases the APC population in BAT through the key factors including *PPARγ*, *C/EBPβ*, and *BMP7*. As shown in Supplemental Figure S1, the expression of *PPARγ*, *C/EBPβ*, and *BMP7* were all decreased in HFD-fed mice as compared with the ND-fed mice, although no significant differences were found in this study.

HFD induced changes in adipose tissue gene and protein expression

To assess the alterations of adipose-related gene expression in HFD-induced obesity, we compared the expression of 9 genes which expressed in brown or white adipocytes (Jogie-Brahim et al., 2009; Lin and Li, 2004; Westerberg et al., 2006; Wolf, 2009; Wu and Boss, 2007) from the ND- and HFD-fed mice. As expected, HFD-treated mice showed an increase in the expression of genes encoding UCP1 in interscapular brown adipose tissue when compared with the ND group (Fig. 4B). Nevertheless, there were no significant alterations of this gene expression in the perivascular BAT between these two groups with different diet (Fig. 4D). The expression of *Pgc-1α* (PPAR gamma coactivator 1α) and *Prdm16* (a master regulator of brown adipocyte specification and differentiation) were low in the interscapular

and perivascular fat tissues (Fig. 4B, D). Likewise, we did not find any significant difference in *Elovl3* (an elongase enzyme important for elongation of monounsaturated or saturated very long chain fatty acids), or *CPT-1M* (Carnitine palmitoyltransferase 1 muscle isoform), both of which were expressed at a very low level (Fig. 4B, D). Except for the inguinal white adipose tissue, these brown adipocyte-specific genes were detected in the epididymal and retroperitoneal white adipose tissues (Fig. 4A, C, E). *Cidea* (a lipid droplet-associated protein with a role in fat storage) gene expression was decreased in HFD-fed mice than ND-fed mice in the white adipose tissue (Fig. 4A, C, E). Dermatopontin (*DPT*), insulin-like growth factor binding protein 3 (*Igfbp3*), homeobox C9 (*Hoxc9*), the specific genes for white adipose tissue were expressed at a very low level in brown adipose tissue, whereas there was no significant difference between ND and HFD groups (Fig. 4A–E). Consistent with *Ucp1* gene expression, data from Western blotting (Fig. 5A–B) and immunohistochemistry (Fig. 5C–D) also demonstrated a significant increase in UCP1 protein level in interscapular brown adipose tissue depot, although it was undetectable in white inguinal, epididymal and retroperitoneal adipose depots at protein levels.

Vasomotor responses

To investigate the role of brown adipose tissue surrounding the vessels in response to HFD, functional study with mice aorta was examined in the presence and absence of perivascular adipose tissue. Mice fed a ND displayed a comparable relaxation response to acetylcholine (Fig. 6A) and a constriction response to phenylephrine (Fig. 6B) with and without perivascular fat tissue. However, in mice fed a HFD, greater vasorelaxation was shown in aortic rings without adipose tissue than those with adipose tissue (Fig. 6A). Consistent with this, constriction in response to phenylephrine was less in rings without perivascular adipose tissue than with the adipose tissue (Fig. 6B). As shown in Fig. 6A, HFD-fed mice exhibited an attenuated relaxation response to acetylcholine compared with the mice fed a ND only in the presence of perivascular fat tissue, although we did not observe significant difference between these 2 groups. These data, collectively, indicate an important role for perivascular fat in mediating response to a HFD.

Superoxide production

We then measured the superoxide production in the aorta in response to HFD due to the evidence that oxidative stress contributes to mechanisms of vascular dysfunction (Heitzer et al., 2001; Miller et al., 1998). Morphologic analysis revealed intracellular formation of O_2^- documented by DHE oxidation in vessel area (Fig. 7). Quantification of the fluorescent signal showed a significant increase in fluorescence in the vessels of HFD group when compared with the control ND arteries ($2.42 \pm 0.45\%$ *vs.* $0.87 \pm 0.63\%$, $p < 0.01$).

Adiponectin and AMPK

To further define the possible underlying mechanisms, we measured the adiponectin level and AMPK activity. As shown in Fig. 8A–C, circulating adiponectin as well as liver adiponectin was significantly reduced by HFD feeding when compared with mice fed ND, although we did not find any significant difference in the level of adiponectin in the visceral adipose tissue. Next, we measured the AMPK expression in the liver. As shown in Fig. 8D–E, The ratio of phopho-AMPKα to AMPKα was significantly lower in the HFD-fed mice than in the ND-fed mice.

Discussion

In this study, we evaluated the changes at cellular, functional, and genetic levels in brown and white adipose tissues in response to long-term HFD intervention. To our knowledge, this is the first study to evaluate the effect of long-term high-fat intake on APC population in

both BAT and WAT in a high-fat diet-induced mouse model. There are several important findings in this study. Firstly, long-term HFD decreased adipocyte progenitor population in brown adipose. Secondly, HFD feeding increased UCP1 expression in BAT. Thirdly, HFD feeding results in altered vascular function related with perivascular adipose tissue and increased superoxide production. Finally, adiponectin-AMPK signaling might be involved in the adverse effect of chronic high-fat intake.

It is well known that obesity is characterized by increased adipose tissue mass. Actually, adipose tissue development begins during gestation in higher mammals and shortly after birth in rodents (Crossno et al., 2006). With appropriate stimulation, the preadipocytes undergo adipogenic conversion to mature, lipid-filled, insulin-sensitive adipocytes. After birth and throughout life, adipose tissue can expand in response to elevated dietary energy intake via hypertrophy of existing fat cells and through the generation of new adipocytes (hyperplasia). Adipocyte hypertrophy is largely due to the accumulation of additional triglyceride from dietary sources (Garaulet et al., 2006), which is verified in our study. Because the mature adipocytes are postmitotic, hyperplastic growth should be attributed to the differentiation of preadipocytes. In this study, the flow cytometric data demonstrated a decrease in APC number in BAT from mice fed a HFD, whereas no difference was observed in WAT between mice fed a HFD or ND. Thus, the enlarged fat size might, at least partially explain the increased fat mass. In addition, the new adipocytes arise not only from resident preadipocyte progenitors, but also from mesenchymal progenitor cells and nonresident preadipocytes (bone marrow-derived progenitor cells) (Crossno et al., 2006). Whether the progenitor cells from mesenchymal and bone marrow is involved the increased adipose tissue needs to be further investigated. In contrast, findings from an earlier study (Xu et al., 2011), which only investigated APC in brown adipose tissue, demonstrated that HFD did not induce significant change in BAT. This discrepancy may be explained by differences in the time of feeding duration. In this study, the mice were fed a HFD for about 8 months; however, the previous study was focused on the animals with 8-week HFD feeding.

Energy balance to prevent the development of obesity is dependent on energy expenditure. Although physical activity is the dominant mechanism for dissipating excess energy, the uncoupling of oxidative phosphorylation in brown adipocytes by mitochondrial UCP1 plays a pivotal role to protect the body from hypothermia (Kozak and Anunciado-Koza, 2008). The increased *Ucp1* mRNA expression and UCP1 protein level in BAT is in agreement with previous studies (Rippe et al., 2000), supporting a role for BAT thermogenesis during HFD feeding. According to the new statistic data, UCP1 expression is positively regulated by feeding a HFD in 42 of 62 studies; 11 of 62 show no effect and 9 of 62 even report a decrease (Fromme and Klingenspor, 2011). Since the same samples were used to test UCP1 mRNA and protein levels in this study, our data adds another definitely positive regulation of UCP1 by long-term intake of HFD. Recent studies showed the expression of UCP1 is not strictly limited to brown adipose tissue, but also found in white fat pads to an extent influenced by the ambient temperature (Rippe et al., 2000). It is known that high caloric intake leads to an increased sympathetic tone (Schwartz et al., 1983), activating UCP1 mediated, adrenergically controlled nonshivering thermogenesis in brown adipocytes (Rothwell and Stock, 1979). Unfortunately, of epididymal, retroperitoneal and inguinal white adipose tissue in this study, only detectable amount of *Ucp1* mRNA were seen in control and HFD conditions. Thus, a “browning” of white fat was not found in this study. *Cidea*, a highly expressed gene in BAT, was reported to decrease in energy expenditure and is resistant to obesity induction (Lin and Li, 2004). Consistent with this, *Cidea* gene expression decreased in response to a HFD, despite no significant difference was shown. However, *Cidea* seems not highly strict to BAT, as it was also detected in epididymal, retroperitoneal, and inguinal fat depots. Since *Cidea* appears to be negatively regulated by HFD both in BAT and WAT, it offers a new option to explore the linkage with obesity,

although the precise mechanism by which *Cidea* regulates energy homeostasis requires further investigation.

Adipose tissue depots are functionally diverse and modulate disease processes in a depot-specific manner. Nevertheless, the functional properties of perivascular adipocytes and their influence on the blood vessel are yet to elucidate. Besides serving largely as structural support for the vasculature, perivascular fat is widely accepted to release an adventitium-derived relaxing factor (Lohn et al., 2002). The vascular tone was regulated by the factor via activating tyrosine kinase-dependent K^+ channels in vascular smooth muscle cells (Lohn et al., 2002) or releasing a potent nitric oxide and prostacyclin-independent anticontractile factor (Malinowski et al., 2008). The initial purpose of this vascular study was to test the hypothesis that perivascular adipose tissue has an anticontractile effect comparable with the reported results (Lohn et al., 2002; Malinowski et al., 2008) in artery from animals fed a ND. However, our results indicate that the adipose tissue has little effect on the relaxant response to acetylcholine or constriction response to phenylephrine in aortic ring preparations from mice with a ND. Although artery rings with intact perivascular fat, from different species of rat or human, blunted constriction in response to serotonin, angiotensin II, endothelin or phenylephrine (Lohn et al., 2002; Malinowski et al., 2008), similar effects to ours was found by Reifenberger *et al* (Reifenberger et al., 2007) in that the presence of perivascular fat or not induced no difference in vasoconstriction response in pig coronary with a ND.

We also tested the hypothesis that the perivascular adipose tissue of mice fed a HFD would exhibit less of a blunting effect on constriction than mice on a ND. Of interest, our results indicated deleterious effects (i.e., greater constriction responses or attenuated relaxant effects) of HFD in the effect of perivascular adipose tissue on artery vasomotor function. In the present study, we did observe that response to KCl were not different in the aorta between ND and HFD, with or without fat. Thus, examining response to high concentration KCl is a standard part of characterizing vasoconstrictor properties of arteries. Henrichot *et al* (Henrichot et al., 2005) demonstrated that perivascular adipose tissue has strong chemotactic activity that is mainly mediated by the secretion of IL-8 and MCP-1. This is of particular interest because both chemokines can induce smooth muscle cell proliferation (Viedt et al., 2002; Yue et al., 1994) and expression of functional chemokine receptors in vascular smooth muscle cells and endothelial cells (Murdoch and Finn, 2000). In the present study, we did not examine the chemokine levels in adipose tissue, but it hints perivascular-derived chemokines may inhibit the secretion of the adipose-derived relaxing factor or counteract its relaxant effect. The increased O_2^- and perivascular-derived chemokines are possible to explain the altered vasomotor function in our study. Hence, our findings suggest that changes in diet-regulated perivascular adipose depots may contribute to the progression of obesity-associated vascular complications.

AMPK, a kinase that phosphorylates and inactivates acetyl coenzyme-A carboxylase (ACC) in fatty acid biosynthesis (Stapleton et al., 1994), is considered a major metabolic regulator at both cellular and whole-body levels (Xu et al., 2011) . After binding with AMP, AMPK was activated via conformational changes that allow Thr172 phosphorylation to occur by upstream kinases. Activation of AMPK in the liver, skeletal muscle, and adipose tissue results in a change of energy utilization involving the stimulation of energy-producing pathways to restore energy balance, thereby improving the status of type 2 diabetes (Yuan et al., 2009). In addition, energy expenditure may also be regulated by AMPK, in which NAD+ metabolism and SIRT1 activity are involved (Canto et al., 2009), rending AMPK as an enzyme central to cellular bioenergetics, AMPK is a ubiquitous heterotrimeric kinase consisting of a catalytic α subunit and regulatory β and γ subunits. The AMPKα subunit is essential, and a dual deficiency in AMPKα1 and AMPKα2 causes embryonic lethality in

mice (Viollet et al., 2009). Adiponectin, a hormone secreted by adipocytes that regulates energy homeostasis and glucose and lipid metabolism, activates AMPK, thereby directly regulating glucose metabolism and insulin sensitivity (Yamauchi et al., 2002). In this study, we showed that HFD feeding induced a decrease in the level of adiponectin in the blood and liver. In addition, AMPK activity, measured as Thr172 phosphorylation, was suppressed in the metabolically active tissues of the mice fed HFD. Consistent with this, it has been reported that HFD reduced the renal AMPK activity (Decleves et al., 2011). These findings suggest that adiponectin-AMPK signaling pathway might be involved in the adverse effect of chronic high-fat intake. Yet, the mechanisms by which HFD selectively decreases the APC population in BAT needs further investigation.

Although this was a long-term HFD intervention that has significant implication in real daily life in humans, especially taking into account of pandemic in overweight and obesity worldwide, there are some limitations in this study. First of all, the detailed mechanisms pertaining aortic vascular response are lacking primarily due to the limitation of aortic rings. Secondly, indirect evidence was provided for the changes in the APC population by flow cytometry. In addition, the sample size was small, and the functional evaluation of brown APC in in-vivo adipogenesis is not available, which is under experiment that is technically challenging.

Conclusions

Chronic high-fat intake not only induces insulin resistance, but also alters APC population and adipose-specific genes in different adipose depots that could have sustained adverse health consequences, in which adiponectin-AMPK signaling might be involved. Moreover, perivascular adipose tissue and increased superoxide production may play a role in HFD-induced vascular dysfunction.

Supplementary Material

Refer to Web version on PubMed Central for supplementary material.

Acknowledgments

This work was supported by National Institute of Health grants ES016588, ES017412, and ES018900 to Dr. Sun and ES015146 to Dr. Rajagopalan.

References

Canto C, Gerhart-Hines Z, Feige JN, Lagouge M, Noriega L, Milne JC, et al. AMPK regulates energy expenditure by modulating NAD+ metabolism and SIRT1 activity. Nature. 2009; 458:1056–60. [PubMed: 19262508]

Conklin BS, Fu W, Lin PH, Lumsden AB, Yao Q, Chen C. HIV protease inhibitor ritonavir decreases endothelium-dependent vasorelaxation and increases superoxide in porcine arteries. Cardiovasc Res. 2004; 63:168–75. [PubMed: 15194474]

Crossno JT Jr, Majka SM, Grazia T, Gill RG, Klemm DJ. Rosiglitazone promotes development of a novel adipocyte population from bone marrow-derived circulating progenitor cells. J Clin Invest. 2006; 116:3220–8. [PubMed: 17143331]

Decleves AE, Mathew AV, Cunard R, Sharma K. AMPK mediates the initiation of kidney disease induced by a high-fat diet. J Am Soc Nephrol. 2011; 22:1846–55. [PubMed: 21921143]

Fromme T, Klingenspor M. Uncoupling protein 1 expression and high fat diets. Am J Physiol Regul Integr Comp Physiol. 2011; 300:R1–8. [PubMed: 21048077]

Gao YJ, Takemori K, Su LY, An WS, Lu C, Sharma AM, et al. Perivascular adipose tissue promotes vasoconstriction: the role of superoxide anion. Cardiovasc Res. 2006; 71:363–73. [PubMed: 16756966]

Garaulet M, Hernandez-Morante JJ, Lujan J, Tebar FJ, Zamora S. Relationship between fat cell size and number and fatty acid composition in adipose tissue from different fat depots in overweight/obese humans. Int J Obes (Lond). 2006; 30:899–905. [PubMed: 16446749]

Heitzer T, Schlinzig T, Krohn K, Meinertz T, Munzel T. Endothelial dysfunction, oxidative stress, and risk of cardiovascular events in patients with coronary artery disease. Circulation. 2001; 104:2673–8. [PubMed: 11723017]

Henrichot E, Juge-Aubry CE, Pernin A, Pache JC, Velebit V, Dayer JM, et al. Production of chemokines by perivascular adipose tissue: a role in the pathogenesis of atherosclerosis? Arterioscler Thromb Vasc Biol. 2005; 25:2594–9. [PubMed: 16195477]

Himms-Hagen J. Brown adipose tissue thermogenesis in obese animals. Nutr Rev. 1983; 41:261–7. [PubMed: 6358959]

Jogie-Brahim S, Feldman D, Oh Y. Unraveling insulin-like growth factor binding protein-3 actions in human disease. Endocr Rev. 2009; 30:417–37. [PubMed: 19477944]

Kozak LP, Anunciado-Koza R. UCP1: its involvement and utility in obesity. Int J Obes (Lond). 2008; 32 (Suppl 7):S32–8. [PubMed: 19136989]

Lane MD, Tang QQ. From multipotent stem cell to adipocyte. Birth Defects Res A Clin Mol Teratol. 2005; 73:476–7. [PubMed: 15959887]

Lin SC, Li P. CIDE-A, a novel link between brown adipose tissue and obesity. Trends Mol Med. 2004; 10:434–9. [PubMed: 15350895]

Liu CQ, Leung FP, Wong SL, Wong WT, Lau CW, Lu L, et al. Thromboxane prostanoid receptor activation impairs endothelial nitric oxide-dependent vasorelaxations: the role of Rho kinase. Biochem Pharmacol. 2009; 78:374–81. [PubMed: 19409373]

Lohn M, Dubrovska G, Lauterbach B, Luft FC, Gollasch M, Sharma AM. Periadventitial fat releases a vascular relaxing factor. Faseb J. 2002; 16:1057–63. [PubMed: 12087067]

Ma L, Ma S, He H, Yang D, Chen X, Luo Z, et al. Perivascular fat-mediated vascular dysfunction and remodeling through the AMPK/mTOR pathway in high-fat diet-induced obese rats. Hypertens Res. 33:446–53. [PubMed: 20186150]

Malinowski M, Deja MA, Golba KS, Roleder T, Biernat J, Wos S. Perivascular tissue of internal thoracic artery releases potent nitric oxide and prostacyclin-independent anticontractile factor. Eur J Cardiothorac Surg. 2008; 33:225–31. [PubMed: 18083040]

Miller FJ Jr, Gutterman DD, Rios CD, Heistad DD, Davidson BL. Superoxide production in vascular smooth muscle contributes to oxidative stress and impaired relaxation in atherosclerosis. Circ Res. 1998; 82:1298–305. [PubMed: 9648726]

Murdoch C, Finn A. Chemokine receptors and their role in inflammation and infectious diseases. Blood. 2000; 95:3032–43. [PubMed: 10807766]

Reifenberger MS, Turk JR, Newcomer SC, Booth FW, Laughlin MH. Perivascular fat alters reactivity of coronary artery: effects of diet and exercise. Med Sci Sports Exerc. 2007; 39:2125–34. [PubMed: 18046183]

Ricquier D. Mitochondrial uncoupling proteins. Curr Opin Drug Discov Devel. 1999; 2:497–504.

Rippe C, Berger K, Boiers C, Ricquier D, Erlanson-Albertsson C. Effect of high-fat diet, surrounding temperature, and enterostatin on uncoupling protein gene expression. Am J Physiol Endocrinol Metab. 2000; 279:E293–300. [PubMed: 10913028]

Rodeheffer MS, Birsoy K, Friedman JM. Identification of white adipocyte progenitor cells in vivo. Cell. 2008; 135:240–9. [PubMed: 18835024]

Rothwell NJ, Stock MJ. A role for brown adipose tissue in diet-induced thermogenesis. Nature. 1979; 281:31–5. [PubMed: 551265]

Schwartz JH, Young JB, Landsberg L. Effect of dietary fat on sympathetic nervous system activity in the rat. J Clin Invest. 1983; 72:361–70. [PubMed: 6874952]

Spiegelman BM, Flier JS. Obesity and the regulation of energy balance. Cell. 2001; 104:531–43. [PubMed: 11239410]

Stapleton D, Gao G, Michell BJ, Widmer J, Mitchelhill K, Teh T, et al. Mammalian 5′-AMP-activated protein kinase non-catalytic subunits are homologs of proteins that interact with yeast Snf1 protein kinase. J Biol Chem. 1994; 269:29343–6. [PubMed: 7961907]

Sun Q, Yue P, Ying Z, Cardounel AJ, Brook RD, Devlin R, et al. Air pollution exposure potentiates hypertension through reactive oxygen species-mediated activation of Rho/ROCK. Arterioscler Thromb Vasc Biol. 2008; 28:1760–6. [PubMed: 18599801]

Sun Q, Yue P, Deiuliis JA, Lumeng CN, Kampfrath T, Mikolaj MB, et al. Ambient air pollution exaggerates adipose inflammation and insulin resistance in a mouse model of diet-induced obesity. Circulation. 2009; 119:538–46. [PubMed: 19153269]

Verhagen SN, Visseren FL. Perivascular adipose tissue as a cause of atherosclerosis. Atherosclerosis. 2011; 214:3–10. [PubMed: 20646709]

Viedt C, Vogel J, Athanasiou T, Shen W, Orth SR, Kubler W, et al. Monocyte chemoattractant protein-1 induces proliferation and interleukin-6 production in human smooth muscle cells by differential activation of nuclear factor-kappaB and activator protein-1. Arterioscler Thromb Vasc Biol. 2002; 22:914–20. [PubMed: 12067898]

Viollet B, Athea Y, Mounier R, Guigas B, Zarrinpashneh E, Horman S, et al. AMPK: Lessons from transgenic and knockout animals. Front Biosci. 2009; 14:19–44. [PubMed: 19273052]

Wainwright MS, Kohli R, Whitington PF, Chace DH. Carnitine treatment inhibits increases in cerebral carnitine esters and glutamate detected by mass spectrometry after hypoxia-ischemia in newborn rats. Stroke. 2006; 37:524–30. [PubMed: 16385097]

Westerberg R, Mansson JE, Golozoubova V, Shabalina IG, Backlund EC, Tvrdik P, et al. ELOVL3 is an important component for early onset of lipid recruitment in brown adipose tissue. J Biol Chem. 2006; 281:4958–68. [PubMed: 16326704]

Wolf G. Brown adipose tissue: the molecular mechanism of its formation. Nutr Rev. 2009; 67:167–71. [PubMed: 19239631]

Wu Z, Boss O. Targeting PGC-1 alpha to control energy homeostasis. Expert Opin Ther Targets. 2007; 11:1329–38. [PubMed: 17907962]

Xu MJ, Song P, Shirwany N, Liang B, Xing J, Viollet B, et al. Impaired expression of uncoupling protein 2 causes defective postischemic angiogenesis in mice deficient in AMP-activated protein kinase alpha subunits. Arterioscler Thromb Vasc Biol. 2011; 31:1757–65. [PubMed: 21597006]

Xu X, Yavar Z, Verdin M, Ying Z, Mihai G, Kampfrath T, et al. Effect of Early Particulate Air Pollution Exposure on Obesity in Mice: Role of p47phox. Arterioscler Thromb Vasc Biol. 2010; 30:2518–27. [PubMed: 20864666]

Xu X, Ying Z, Cai M, Xu Z, Li Y, Jiang SY, et al. Exercise ameliorates high-fat diet-induced metabolic and vascular dysfunction, and increases adipocyte progenitor cell population in brown adipose tissue. Am J Physiol Regul Integr Comp Physiol. 2011; 300:R1115–25. [PubMed: 21368268]

Yamauchi T, Kamon J, Minokoshi Y, Ito Y, Waki H, Uchida S, et al. Adiponectin stimulates glucose utilization and fatty-acid oxidation by activating AMP-activated protein kinase. Nat Med. 2002; 8:1288–95. [PubMed: 12368907]

Yuan H, Shyy JY, Martins-Green M. Second-hand smoke stimulates lipid accumulation in the liver by modulating AMPK and SREBP-1. J Hepatol. 2009; 51:535–47. [PubMed: 19556020]

Yue TL, Wang X, Sung CP, Olson B, McKenna PJ, Gu JL, et al. Interleukin-8. A mitogen and chemoattractant for vascular smooth muscle cells. Circ Res. 1994; 75:1–7. [PubMed: 8013067]

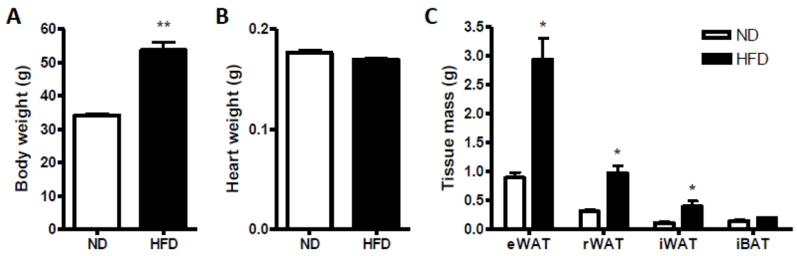

Fig. 1.

Effect of diet intervention with either a normal diet (ND) or high-fat diet (HFD) on body weight gain and tissue mass change. A–B, Effect of HFD on body weight gain (A) and heart weight (B). C, Effect of HFD on fat tissue mass change. eWAT, epididymal white adipose tissue; iWAT, inguinal white adipose tissue; rWAT, retroperitoneal white adipose tissue; iBAT, interscapular adipose tissue. n=4 per group. *$p < 0.05$, **$p < 0.01$ compared with the ND group.

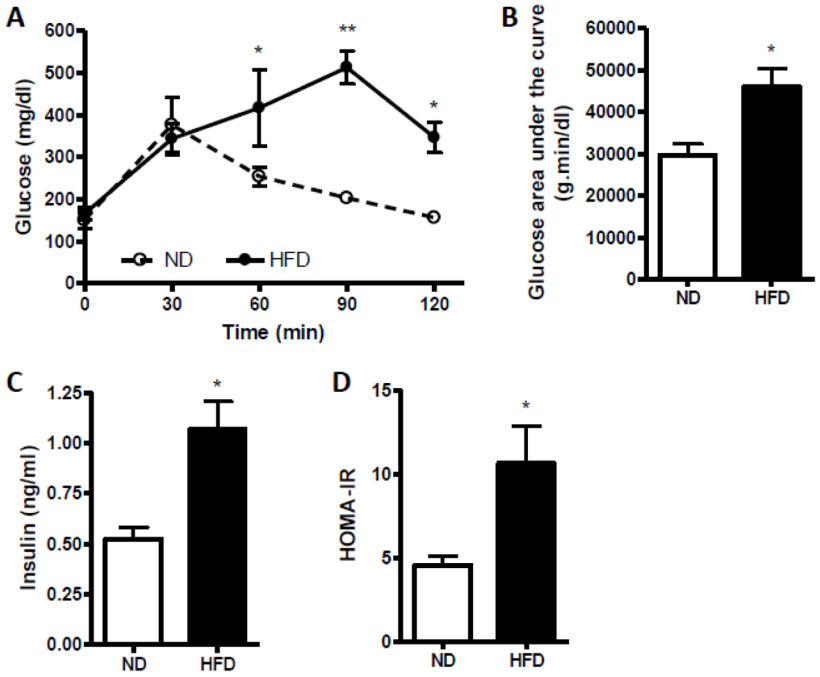

Fig. 2.

Glucose homeostasis in C57BL/6 mice fed a normal diet (ND) or high-fat diet (HFD). A, Effect of HFD on glucose tolerance by intraperitoneal glucose tolerance test (IPGTT). B, Glucose area under the curve calculated from the glucose tolerance test in part A. C, Effect of HFD on fasting plasma insulin level. D, The homeostasis model assessment insulin resistance (HOMA-IR) index. n=4 per group. *$p < 0.05$, **$p < 0.01$ compared with the ND group.

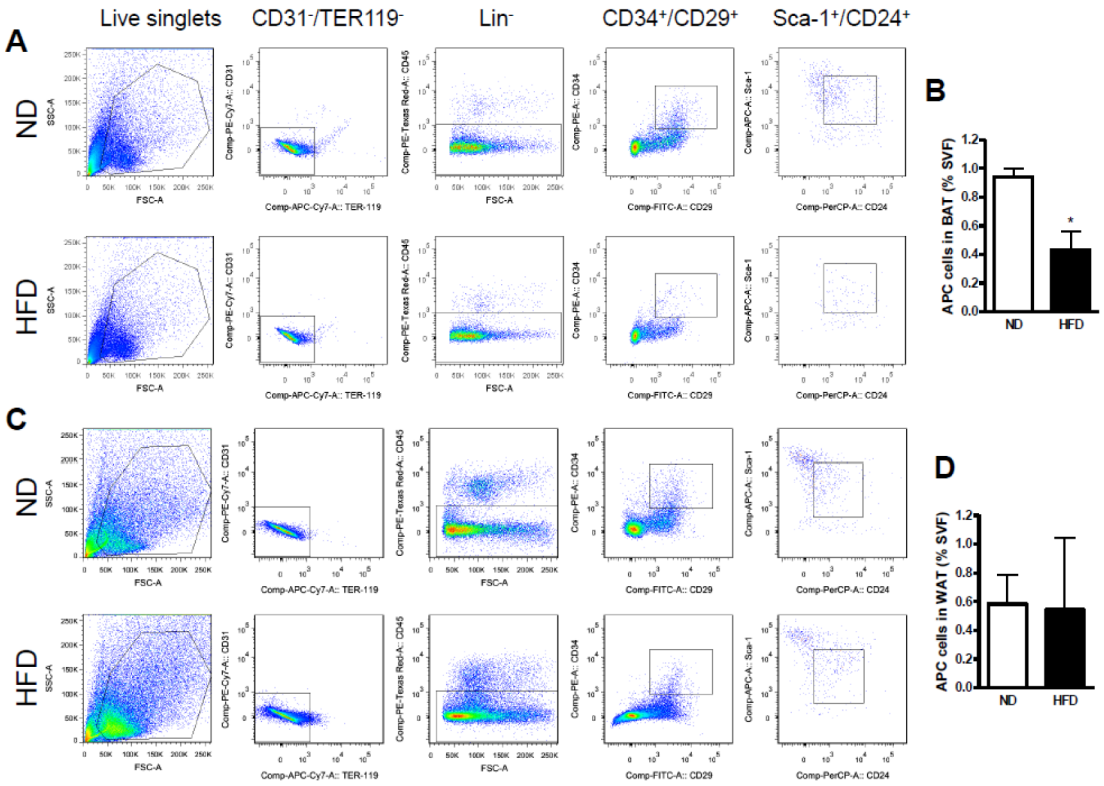

Fig. 3.

Analysis of adipose progenitor cells (APC) by flow cytometry. Identification of adipogenic cell population in adipose stroma from white and brown fat tissues of mice fed a ND or HFD. Cells were initially selected by size, on the basis of forward scatter (FSC) and side scatter (SSC). The live singlets were sorted for lack of CD31 and Ter119 expression, and were further separated on the basis of expression of CD45. $CD45^{-}$ cells (Lin^{-}) were then sorted on the expression of CD34 and CD29. $CD34^{+}$ cells were sorted on the basis of staining for Sca-1 and CD24 (right-hand plot). APC population changes in response to a HFD by flow cytometry in brown adipose tissue (A, B) and white adipose tissue (C, D). n=4 per group. $*p < 0.05$ compared with the ND group.

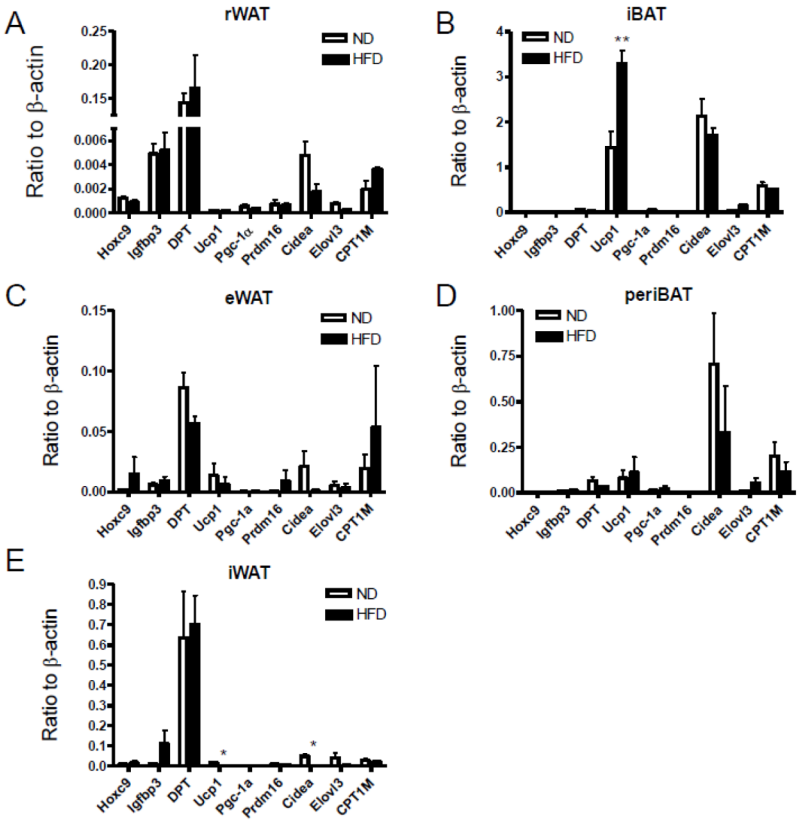

Fig. 4.

Altered expression of adipose-related genes in response to a diet intervention of ND or HFD. Quantitative real-time PCR was used to measure the expression of genes involved energy metabolism in different adipose tissues, including rWAT, retroperitoneal white adipose tissue (A); iBAT, interscapular brown adipose tissue (B); eWAT, epididymal white adipose tissue (C); periBAT, perivascular adipose tissue (D); iWAT, inguinal white adipose tissue (E). n=4 per group. *$p < 0.05$ compared with the ND group.

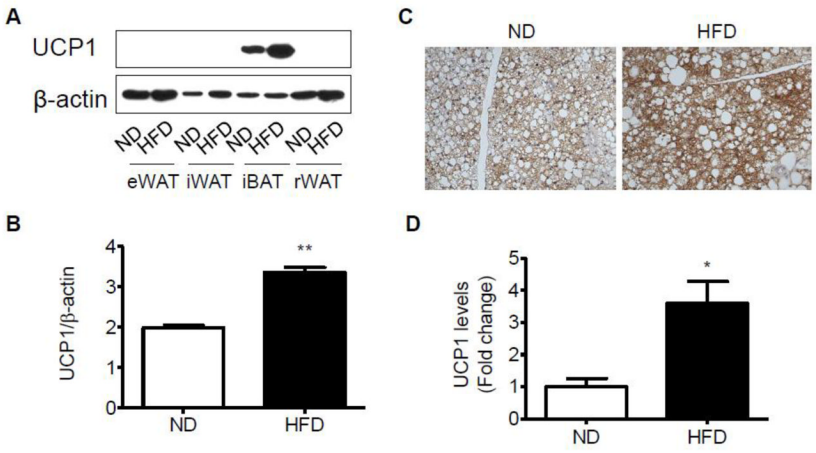

Fig. 5.

Altered expression of UCP1 in response to dietary uptake in the adipose tissues. Representative bands (A) and statistical analysis (B) of Western blotting in different adipose depots of mice fed a ND or HFD. Representative bands (C) and statistical analysis (D) of immunohistochemistry for UCP1 in interscapular adipose tissue for all the mice fed a ND or HFD. n=4 per group. *$p < 0.05$; **$p < 0.01$ compared with the ND group.

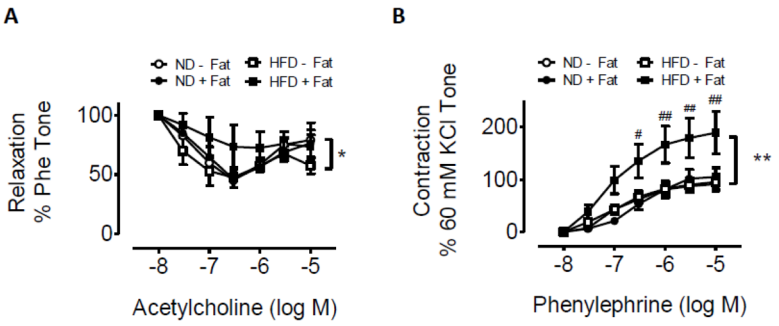

Fig. 6.

Effect of diet intervention with a ND or HFD on vasomotor tone in aortic rings by myography. A, vasomotor tone change in aortic rings with (+fat) or without (−fat) perivascular adipose tissue in response to acetylcholinein ND- and HFD-fed mice. B, vasomotor tone change in aortic rings with (+fat) or without (−fat) perivascular adipose tissue in response to phenylephrine in ND- and HFD-fed mice. n=4 per group. *$p < 0.05$; **$p < 0.01$ compared with the responses of aortic rings without perivascular adipose.

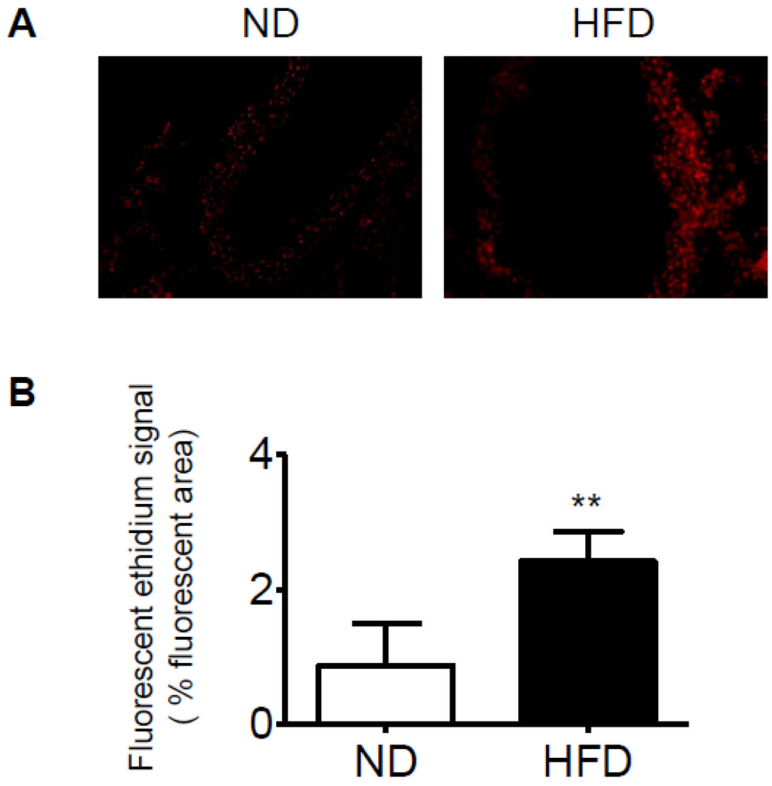

Fig. 7.

Reactive oxygen species (ROS) generation within the aortas from ND- or HFD-fed mice, as determined by dihydroethidium (DHE) fluorescence (100× magnification). Fluorescent photomicrographs at identical settings of sections of thoracic aorta labeled with DHE. A, representative photomicrographs of DHE staining from the mice fed a ND (left) or HFD (right); Bottom, quantification of the fluorescent ethidium signal in the HFD group compared with the ND group. n=4 per group. $^{**}p < 0.01$ compared with the control group.

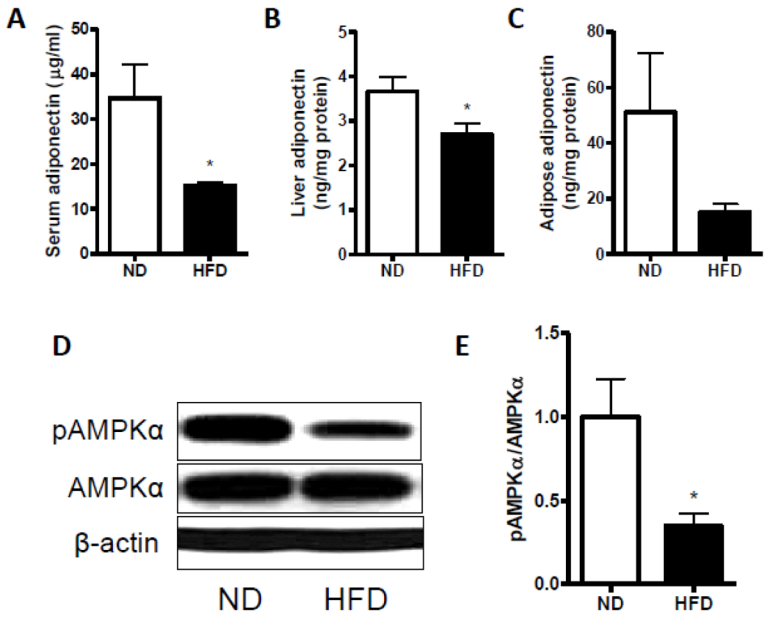

Fig. 8.

Adiponectin and AMPK activity in response to dietary uptake in the adipose tissue. Measurement of adiponectin in blood (A), liver (B), and visceral white adipose tissue (C). Representative bands (D) and statistical analysis (E) of Western blotting for phopho-AMPKα (pAMPKα) and AMPKα in the liver from all the mice fed a ND or HFD. n=4 per group. *$p < 0.05$ compared with the ND group.

Table 1

Primers used for real-time PCR

Primer	Forward oligonucleotides	Reverse oligonucleotides
Hoxc9	5′-GCAGCAAGCACAAAGAGGAGAAG-3′	5′-GCGTCTGGTACTTGGTGTAGGG-3′
Igfbp3	5′-GCAGCCTAAGCACCTACCTC-3′	5′-TCCTCCTCGGACTCACTGAT-3′
DPT	5′-CTGCCGCTATAGCAAGAGGT-3′	5′-TGGCTTGGGTACTCTGTTGTC-3′
Ucp1	5′-ACTGCCACACCTCCAGTCATT-3′	5′-CTTTGCCTCACTCAGGATTGG-3′
Pgc-1α	5′-CCCTGCCATTGTTAAGACC-3′	5′-TGCTGCTGTTCCTGTTTTC-3′
Prdm16	5′-CAGCACGGTGAAGCCATTC-3′	5′-GCGTGCATCCGCTTGTG-3′
Cidea	5′-ATCACAACTGGCCTGGTTACG-3′	5′-TACTACCCGGTGTCCATTTCT-3′
Elovl3	5′-GATGGTTCTGGGCACCATCTT-3′	5′-CGTTGTTGTGTGGCATCCTT-3′
CPT1M	5′-TGCCTTTACATCGTCTCCAA-3′	5′-GGCTCCAGGGTTCAGAAAGT-3′
C/EBPβ	5′-ACGACTTCCTCTCCGACCTCT-3′	5′-CGAGGCTCACGTAACCGTAGT-3′
PPARγ	5′-GCATGGTGCCTTCGCTGA-3′	5′-TGGCATCTCTGTGTCAACCATG-3′
BMP7	5′-AGCTACCACAGCAAACGCCTAAGA-3′	5′-TGAACGAGGCTTGCGATTACTCCT-3′
β-actin	5′-TGTGATGGTGGGAATGGGTCAGAA-3′	5′-TGTGGTGCCAGATCTTCTCCATGT-3′